Dynamic structure of expanded liquid rubidium from a molecular-dynamics simulation

2000 J. Phys.: Condens. Matter 12 4313

(http://iopscience.iop.org/0953-8984/12/19/302)

J. Phys.: Condens. Matter **12** (2000) 4313–4326. Printed in the UK PII: S0953-8984(00)11189-0

Dynamic structure of expanded liquid rubidium from a molecular-dynamics simulation

Shuji Munejiri†, Fuyuki Shimojo and Kozo Hoshino

Faculty of Integrated Arts and Sciences, Hiroshima University, Higashi-Hiroshima 739-8521, Japan

E-mail: munejiri.shuuji@nasda.go.jp

Received 20 January 2000, in final form 28 March 2000

Abstract. The dynamic structures of expanded liquid rubidium from the triple point to near the critical point are investigated by means of a molecular-dynamics simulation with the effective pair potential obtained from the experimental structure factor by the inverse method. The results are discussed in comparison with the experimental data and also with those obtained with the effective pair potential derived by means of the pseudopotential perturbation theory. It is shown that the effective pair potential obtained from the static structure factor can reproduce fairly well the dynamic structure factor for a wide range of density up to near the critical point.

1. Introduction

The structures of expanded liquid alkali metals such as rubidium and caesium have been extensively investigated. These liquid metals show the metal–nonmetal (M–NM) transition, when they are expanded from the triple point up to near the critical point. Since the interatomic interaction of the expanded liquid alkali metal strongly depends on the density, attention has been attracted to the density dependence of the structure of these liquid metals.

Owing to the recent progress in experimental techniques at high temperatures and high pressures, the static structures of expanded liquid rubidium [1, 2] and caesium [3] for a wide range of density have been investigated by means of neutron and x-ray scattering. As for the dynamic properties, Pilgrim *et al* [4–7] have studied the dynamic structure factor of liquid rubidium from near the triple point up to near the critical point by carrying out a neutron inelastic scattering experiment and discussed the change of the dynamic structures with decreasing density in connection with the M–NM transition.

There are also theoretical and molecular-dynamics (MD) studies on the expanded liquid alkali metals with the effective pair potentials derived by means of the pseudopotential perturbation theory. Hoshino *et al* [8–12] studied the density dependence of both the static and the dynamic structures of expanded liquid alkali metals by using the integral equation theory and the viscoelastic approximation. The characteristic features of the observed density dependence of the structure are well reproduced from the triple point up to about three times the critical density. As for the MD study, Kahl and Kambayashi [13, 14] calculated the dynamic structures of expanded liquid rubidium. Their results are in good agreement with experimental data except for the state at high temperature and low density near the critical point.

† Present address: Space Utilization Research Programme, National Space Development Agency of Japan (NASDA), 2-1-1 Sengen, Tsukuba 305-8505, Japan.

0953-8984/00/194313+14$30.00

In any studies with the effective pair potentials based on the pseudopotential perturbation theory, the disagreement between the calculated structure and experimental one becomes larger with increasing temperature and decreasing density. The reason for this is that, since the pseudopotential theory is based on the nearly free-electron model, it is not valid at low density where the M–NM transition occurs. At present, however, there is no theoretical method for deriving the effective pair potential for such states.

On the other hand, Shimojo *et al* [15, 16] studied the structural and electronic properties of expanded liquid rubidium by means of an *ab initio* MD simulation. They showed that the static structures are in good agreement with experiments and that, while near the triple point the electron density spreads over the whole space, at high temperature and low density it tends to localize due to a large spatial fluctuation of the atomic density. Recently, González *et al* [17] have studied the dynamic structure factors of expanded liquid rubidium by means of a so-called orbital-free *ab initio* MD simulation. These days, *ab initio* MD simulations are very powerful tools for studying structures of liquids. However, the system size and the run time of the simulation are restricted, since the methods have an enormous computation cost compared with that for classical MD simulations. Therefore, to study the long-time or long-range correlation functions, the conventional MD simulation is still useful, provided that a reliable interatomic potential is available.

The inverse method, in which the effective pair potential is derived from the experimental static structure factor, is one of the best methods for obtaining the effective pair potential when there is no reliable theoretical method. We derived the effective pair potentials of expanded liquid rubidium [18] and caesium [19] using the predictor–corrector method [20, 21] for the inverse method, and investigated their density dependence. It is obvious from the character of this method that these effective pair potentials can reproduce the experimental static structure factors accurately for any states. However, it is not evident that such an effective pair potential can also reproduce the dynamic structure of expanded liquid metals. There are some examples of this kind of study; Dzugutov and Dahlborg [22] studied the dynamic properties of liquid bismuth near its melting point using the effective pair potential derived from the experimental structure factor. In their method, the parametrized phenomenological form of the effective pair potential was optimized iteratively so as to reproduce the experimental static structure factor. They demonstrated that the results for the dynamic structure factors are in good agreement with the experimental data. Recently we [23] studied the density dependence of the velocity of sound in expanded liquid mercury with the effective pair potential obtained by the inverse method and clarified the relation between the effective pair potential and the velocity of sound.

In this study [24] we investigate the dynamic structures of expanded liquid rubidium for three states, at 350, 1700 and 1900 K, from the triple point up to near the critical point, by means of a MD simulation using two kinds of effective pair potential, $\phi_{ps}(r)$ and $\phi(r)$; $\phi_{ps}(r)$ is the one obtained from the pseudopotential perturbation theory using the HHWY pseudopotential given by Hasegawa *et al* [25] and the local-field correction due to Ichimaru and Utsumi [26], and $\phi(r)$ is the one derived from the experimental structure factor by the inverse method [18]. These effective pair potentials are shown in figure 1. The results for the dynamic properties obtained by means of the MD simulation with $\phi_{ps}(r)$ and $\phi(r)$ will be compared with each other and also discussed in connection with the neutron inelastic experiments. At near the triple point, 350 K, the dynamic properties obtained with $\phi_{ps}(r)$ are in good agreement with experimental data [11, 13, 14]. Since, however, there are some discrepancies between $\phi_{ps}(r)$ and $\phi(r)$, we investigate to what extent the difference between the effective pair potentials affects the dynamic properties. The dynamic structures at 1700 and 1900 K are studied for the following reasons. First, Kahl and Kambayashi [13] showed in their MD study that quantitative discrepancies between the results obtained with $\phi_{ps}(r)$ and the experiment are seen at higher

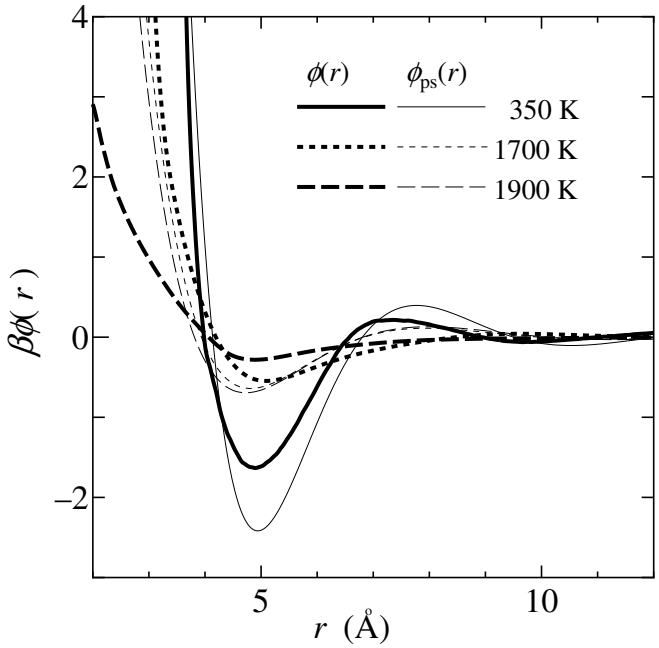

Figure 1. The effective pair potentials multiplied by $\beta = 1/k_B T$ of expanded liquid rubidium at 350 K (solid line), 1700 K (broken line) and 1900 K (dashed line), derived by the inverse method (thick lines) and from the pseudopotential theory (thin lines).

temperatures than 1673 K. Second, not only quantitative differences between them but also qualitative discrepancies are found at 1873 K; Pilgrim *et al* [5–7] observed in their neutron inelastic scattering experiment that a side peak emerges near 4.5 ps^{-1} for wavevectors around 1.0 $Å^{-1}$ in the dynamic structure factor and attributed the side peak to a vibration mode of a rubidium dimer. However, it is known that $\phi_{ps}(r)$ cannot reproduce not only the dynamic structure but also the static structure of this thermodynamic state especially in the small-k region. Under these circumstances, it is interesting to study whether $\phi(r)$ can reproduce the characteristic feature of the dynamic structure at high temperature and high pressure. The purpose of this study is to investigate how the effective pair potential derived from the experimental static structure factor can reproduce the experimental dynamic properties of expanded liquid rubidium for a wide range of density, in particular, at high temperature and high pressure near the critical point.

2. Method of calculation

For convenience, the definitions of some space-time correlation functions are briefly summarized [27]. The intermediate-scattering function $F(k, t)$ is defined as the space Fourier transform of the Van Hove correlation function $G(r, t)$:

$$F(k,t) = \int \mathrm{d}\boldsymbol{r}\ \exp(-\mathrm{i}\boldsymbol{k}\cdot\boldsymbol{r})G(r,t) \tag{1}$$

or

$$F(k,t) = \frac{1}{N}\langle n_{\boldsymbol{k}}(t)n_{-\boldsymbol{k}}(0)\rangle \tag{2}$$

where

$$n_{\boldsymbol{k}}(t) = \sum_{j=1}^{N} \exp(\mathrm{i}\boldsymbol{k} \cdot \boldsymbol{r}_j(t)) \tag{3}$$

is the Fourier transform of the density operator, $\langle \cdots \rangle$ means thermal average and N is the number of atoms. The dynamic structure factor $S(k, \omega)$ is given as

$$S(k, \omega) = \int \mathrm{d}t \ \exp(-\mathrm{i}\omega t) F(k, t). \tag{4}$$

$S(k, \omega)$ gives the frequency spectrum of the correlation between density fluctuations of a given wavevector. We note that

$$\frac{1}{2\pi} \int \mathrm{d}\omega \ S(k, \omega) = F(k, 0) = S(k) \tag{5}$$

is the static structure factor. The self-diffusion coefficient D is obtained from the relation

$$D = \frac{1}{6t} \left\langle r^2(t) \right\rangle \tag{6}$$

where $\left\langle r^2(t) \right\rangle$ is the mean square displacement (MSD) of atoms. This expression for D, which is a time-independent quantity, should be applied to the time region where $\left\langle r^2(t) \right\rangle$ varies linearly with t. In a fluid system, the linear behaviour in $\left\langle r^2(t) \right\rangle$ is obtained at much longer time compared with the characteristic time of correlation between the tagged atom and its immediate neighbours. Therefore equation (6) is valid only for large t. The velocity autocorrelation function $Z(t)$ is defined by

$$Z(t) = \frac{1}{N} \sum_{j=1}^{N} \langle \boldsymbol{v}_j(t) \cdot \boldsymbol{v}_j(0) \rangle \tag{7}$$

where $\boldsymbol{v}_j(t)$ is the velocity of the jth atom at time t.

The constant-temperature MD simulation [28] is performed with periodic boundary conditions. The equations of motion are integrated by the velocity Verlet algorithm. We take 512 atoms in a cubic cell with a side of L for all states and also employ 8000 atoms for the state at the temperature of 1900 K to obtain the long-range correlation functions. The simulation is carried out for 110 000 time steps with the increment of time $\Delta t = 4.8$ fs. The dynamic properties are obtained using the data for 100 000 steps, i.e. 480 ps, after the equilibrium is reached. The cut-off distance of the effective pair potential is given in table 1. To avoid the truncation error in the Fourier transform, $F(k, t)$ is calculated not from equation (1) but from equation (2). The dynamic structure factor $S(k, \omega)$ is calculated by the Fourier

Table 1. Correspondence between experiments and the present study. The cut-off distances r_c for the effective pair potentials $\phi(r)$ and $\phi_{ps}(r)$ employed in our simulation are also shown.

Experiment			Present study			
					r_c (Å)	
T (K)	ρ (g cm^{-3})	Reference	T (K)	ρ (g cm^{-3})	$\phi(r)$	$\phi_{ps}(r)$
315, 320	—	[30,31]	350	1.459	14.0	17.0
1673	0.830	[4]	1700	0.798	14.0	14.0
1873	0.640	[4]	1900	0.642	18.0	18.0

transformation of $F(k,t)$ as defined by equation (4). The wavevector k is restricted by the periodic boundary condition as

$$k = |\boldsymbol{k}| = \left|\frac{2\pi}{L}(n_1, n_2, n_3)\right| \tag{8}$$

where n_1, n_2, n_3 are integers. When $F(k,t)$ or $S(k,\omega)$ is calculated, the average is taken over all equivalent possible vectors $\boldsymbol{k}$ with $k = |\boldsymbol{k}|$.

3. Results and discussion

3.1. Static structure factors

The static structure factor is calculated by the Fourier transformation of the extrapolated $g(r)$; since $g(r)$ available from the MD simulation is limited to $r < L/2$, $g(r)$ is extrapolated beyond $r = L/2$ by Verlet's extrapolation method [29]. In figure 2, thus-obtained and experimental structure factors $S(k)$ of liquid rubidium at 350, 1700 and 1900 K are shown. The solid and the dashed lines show the results obtained from the MD simulation with $\phi(r)$ and $\phi_{ps}(r)$,

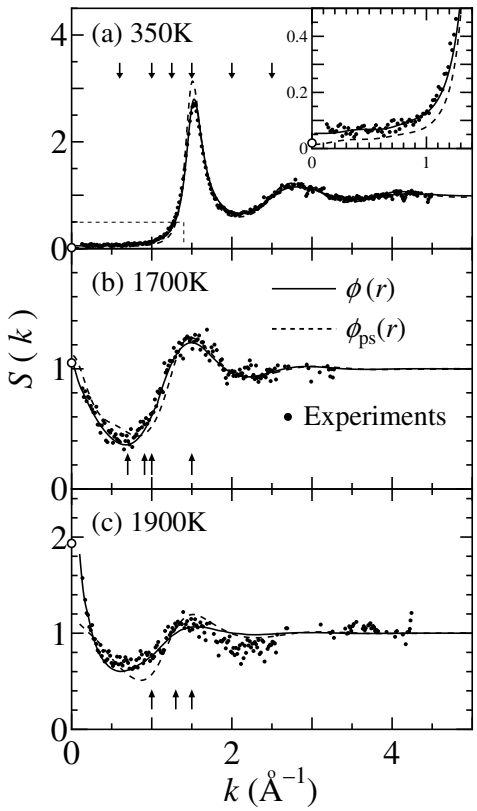

Figure 2. The static structure factors of expanded liquid rubidium at 350 K (a), 1700 K (b) and 1900 K (c). The solid and dashed lines show the results obtained from the MD simulation with $\phi(r)$ and $\phi_{ps}(r)$, respectively. The dots show the experimental data. The open circle is the value of $S(0)$ estimated from the observed isothermal compressibility. The arrows show the wavevectors where the dynamic correlation functions are studied in the present paper.

respectively, and the dots show the neutron scattering data [1]. For closer comparison, $S(k)$ in the small-k region is also shown in figure 2(a). At 350 K, the value of $S(0)$ estimated from the experimental isothermal compressibility χ_T, which is shown by the open circle in figure 2(a), is about 0.02. If the original structure data are smoothed, however, the resulting line gives the larger value of $S(0) \simeq 0.05$. Thus, since the experimental structure data in the small-k region are inconsistent with the observed χ_T, the data in such k-regions are not reliable. For this reason, though $S(k)$ obtained with $\phi_{ps}(r)$ disagrees with the experimental data in the region of k less than the value for the first peak k_p, we cannot judge which effective pair potential is better without more accurate experimental data.

The structure factors $S(k)$ at 1700 K are shown in figure 2(b). The $S(k)$ obtained with $\phi(r)$ agrees with the experiment for all k-values. On the other hand, some discrepancies are seen for the $S(k)$ obtained with $\phi_{ps}(r)$ in the region of k less than the value for the first peak position.

The static structure factors $S(k)$ at 1900 K are compared in figure 2(c). Since the experimental data are substantially scattered, we cannot say that for $k > 1.2$ Å^{-1} the solid line is in better agreement with the experiment than the dashed one. On the other hand, for the regions $k \sim 1.0$ Å^{-1} and $k < 0.5$ Å^{-1} we can see that $S(k)$ obtained with $\phi(r)$ agrees with the experiment much better than that obtained with $\phi_{ps}(r)$ does.

In the following, the dynamic structures for k-values shown by the arrows in figure 2 are studied.

3.2. Intermediate-scattering functions

The normalized intermediate-scattering functions $F(k,t)/F(k,0)$ at 350, 1700 and 1900 K are shown in figures 3, 4 and 5, respectively. The solid and the dashed lines are the results

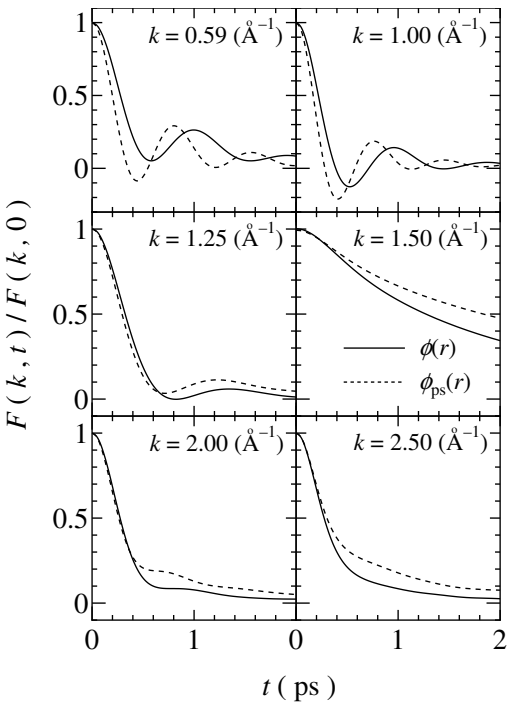

Figure 3. The normalized intermediate-scattering functions $F(k,t)/F(k,0)$ for six wavevectors at 350 K. The solid and dashed lines are the results obtained with $\phi(r)$ and $\phi_{ps}(r)$, respectively.

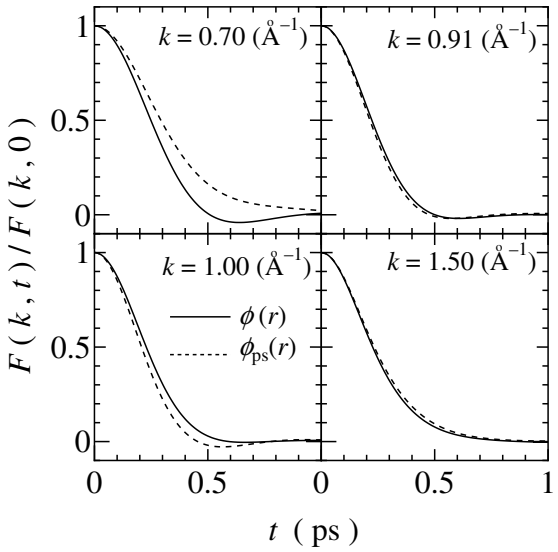

Figure 4. The normalized intermediate-scattering functions $F(k,t)/F(k,0)$ for four wavevectors at 1700 K. The solid and dashed lines are the results obtained with $\phi(r)$ and $\phi_{ps}(r)$, respectively.

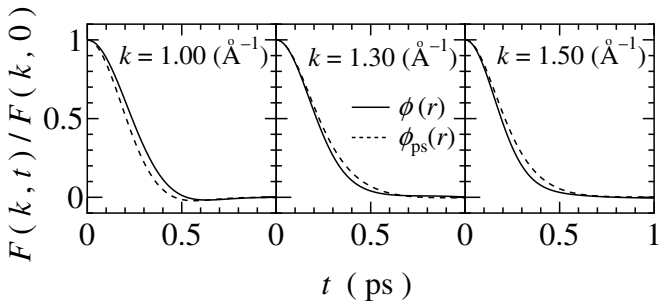

Figure 5. The normalized intermediate-scattering functions $F(k,t)/F(k,0)$ for three wavevectors at 1900 K. The solid and dashed lines are the results obtained with $\phi(r)$ and $\phi_{ps}(r)$, respectively.

obtained from $\phi(r)$ and $\phi_{ps}(r)$, respectively.

At 350 K, the $F(k,t)/F(k,0)$ for $0.3 \leqslant k \leqslant 5.5$ Å^{-1} are calculated with $\phi(r)$ and $\phi_{ps}(r)$ and six of them are shown in figure 3. $F(k,t)$ for k-values less than 1.2 Å^{-1} damps with clear oscillating behaviour. With increasing k, the oscillation tends to damp and $F(k,t)$ for $k \geqslant 1.5$ Å^{-1} decreases monotonically. Because of the strong spatial correlation in the vicinity of k_p ($\sim$1.5 Å^{-1}), $F(k,t)$ decays very slowly at these wavelengths and this behaviour is known as the de Gennes slowing down [32]. Comparing the results obtained with $\phi(r)$ and $\phi_{ps}(r)$, we can see that the period of the oscillation for small k is very sensitive to the effective pair potential. Even if there is little discrepancy between two static structure factors $S(k)$ in a small-k region, $F(k,t)$ in this k-region shows distinctly different behaviours. For the large-k region, though the behaviours of the two $F(k,t)$ are similar, $F(k,t)$ obtained with $\phi_{ps}(r)$ decays more slowly than that obtained with $\phi(r)$. This is because the spatial correlation for the system of atoms interacting with $\phi_{ps}(r)$ is stronger than that for the system interacting with $\phi(r)$.

Figure 4 shows $F(k,t)/F(k,0)$ at 1700 K for four wavevectors. For $k = 0.70$ Å^{-1}, $F(k,t)$

calculated with $\phi(r)$ oscillates and takes negative values at short time, while $F(k, t)$ calculated with $\phi_{ps}(r)$ decays monotonically. In contrast, for $k = 1.00$ Å^{-1}, $F(k, t)$ calculated with $\phi_{ps}(r)$ shows oscillating behaviour, while $F(k, t)$ calculated with $\phi(r)$ decreases monotonically. For the other wavevectors, the $F(k, t)$ calculated with $\phi(r)$ and $\phi_{ps}(r)$ agree with each other very well. For those k-vectors where the $S(k)$ calculated with $\phi(r)$ and $\phi_{ps}(r)$ agree with each other, a good agreement is also achieved for $F(k, t)$.

In figure 5 the $F(k, t)/F(k, 0)$ at 1900 K for $k = 1.00$, 1.30 and 1.50 Å^{-1} are shown. It is reported that the observed $S(k, \omega)$ at 1900 K for $k = 1.0$ Å^{-1} has a peak. Though, in that case, the corresponding $F(k, t)$ is expected to have some oscillating behaviours, our results do not oscillate, but decay monotonically.

3.3. Dynamic structure factors

The dynamic structure factors at 350, 1700 and 1900 K are calculated from the Fourier transforms of $F(k, t)$ shown in figures 3, 4 and 5, respectively. In figure 6 we show the results at 350 K and the neutron inelastic scattering data observed at 315 K and 320 K by Copley and Rowe [30, 31]. For $k \leqslant 1.2$ Å^{-1} clear peaks at finite ω in $S(k, \omega)$ are seen, while for $k \geqslant 1.3$ Å^{-1} no such peak is found. For $k = 1.30$ Å^{-1}, $S(k, \omega)$ for $\phi(r)$ decreases

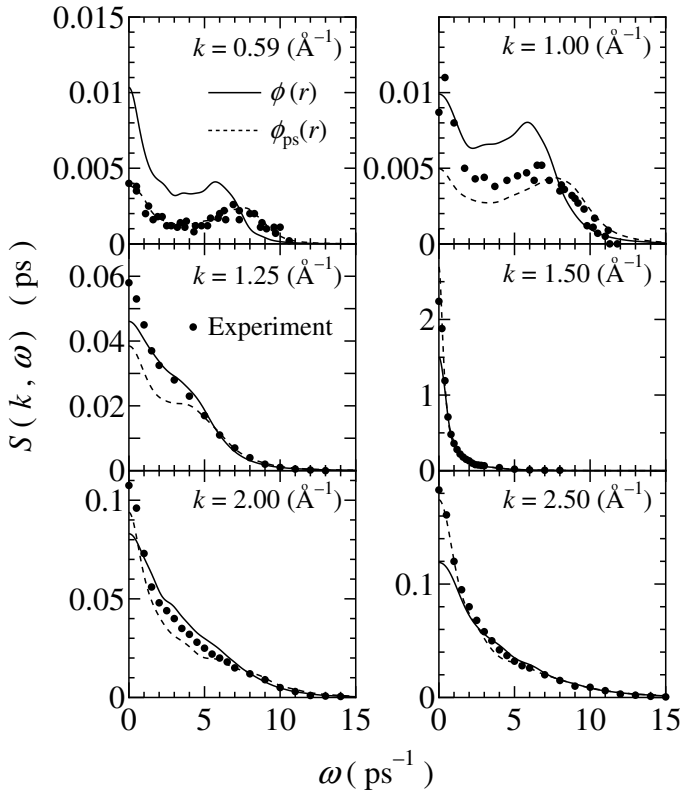

Figure 6. Dynamic structure factors $S(k, \omega)$ at 350 K for the six wavevectors obtained by the Fourier transformation of $F(k, t)$ in figure 3. The solid and dashed lines are the results obtained with $\phi(r)$ and $\phi_{ps}(r)$, respectively. The dots are the neutron inelastic scattering results at 315 and 320 K [30, 31].

monotonically while $S(k, \omega)$ for $\phi_{ps}(r)$ has a shoulder around 3.5 ps^{-1}. $S(k, \omega)$ in the vicinity of k_p has an extremely sharp peak at $\omega = 0$. This behaviour corresponds to the de Gennes narrowing. In the same way as for $F(k, t)$, for the small-k region the two $S(k, \omega)$ obtained with $\phi(r)$ and $\phi_{ps}(r)$ show different behaviours. For $k = 0.59$ $Å^{-1}$ the dashed line is in better agreement with the experiment. This is because, as mentioned above, the experimental static structure factors used as the input data in the inverse method do not have good accuracy in such k-regions. Such a small error in the small-k region has a substantial effect on the effective pair potential, and the resultant dynamic structure for small k disagrees with experiment. For $k = 1.00$ $Å^{-1}$ both the solid and dashed lines disagree with the experimental result. For $k = 1.25$ $Å^{-1}$ the solid line is in better agreement with experiment than the dashed line is. For this k, $S(k)$ obtained with $\phi_{ps}(r)$ disagrees with the experiment. For a larger k, since the errors in the experimental static structure factor are not so serious as that for small k, the two lines show similar behaviours and agree reasonably well with experiments.

In figure 7 we show the dynamic structure factors $S(k, \omega)$ at 1700 K. In the same way as for $F(k, t)$, relatively large discrepancies between $S(k, \omega)$ obtained with $\phi(r)$ and that obtained with $\phi_{ps}(r)$ are seen at the wavevectors $k = 0.70$ and 1.00 $Å^{-1}$ where $S(k)$ obtained with $\phi_{ps}(r)$ and that obtained with $\phi(r)$ disagree with each other. These disagreements can be understood from the sum rule for $S(k, \omega)$ given by equation (5); the larger the $S(k)$ is for a given k, the larger the $S(k, \omega)$ is in the small-ω region. For this thermodynamic state, no side peak is seen for all k-values studied in the present system, while, at 350 K near the triple point, a clear peak at a finite value of ω as well as a sharp peak at $\omega = 0$ can be seen for up to about 1.20 $Å^{-1}$. The experimental dynamic structure factor obtained with the inelastic neutron scattering at 1673 K for $k = 1.0$ $Å^{-1}$ [4, 5] is shown in figure 7. Compared with the experimental data, $S(k, \omega)$ obtained with $\phi_{ps}(r)$ is small near $\omega = 0$. This is because $S(k)$ obtained with $\phi_{ps}(r)$ for $k = 1.00$ $Å^{-1}$ is smaller than the experimental static structure factor. On the other hand, $S(k, \omega)$ obtained with $\phi(r)$ is in excellent agreement with the experiment for the whole ω-region.

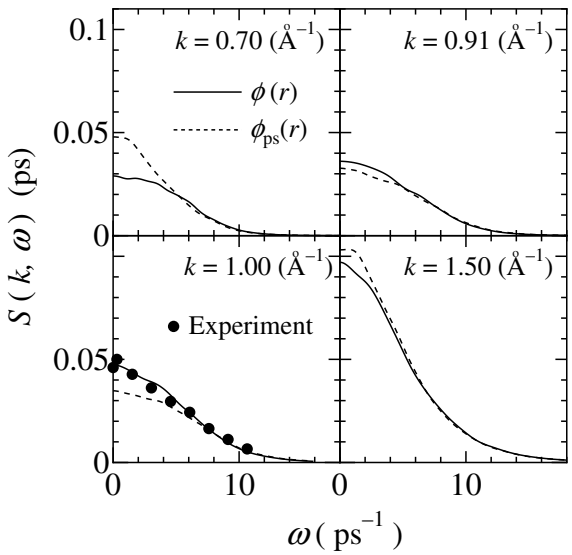

Figure 7. Dynamic structure factors $S(k, \omega)$ at 1700 K for the four wavevectors obtained by the Fourier transformation of $F(k, t)$ in figure 4. The dots are the neutron inelastic scattering results at 1673 K [4].

In figure 8, the $S(k, \omega)$ at 1900 K for $k = 1.00$, 1.30 and 1.50 Å^{-1} are shown. For comparison, the experimental dynamic structure factors obtained by Winter *et al* [6] at 1873 K for $k = 1.0$ Å^{-1} and $k = 1.5$ Å^{-1} are also shown. Comparing with the experimental results for $k = 1.0$ Å^{-1}, we can see that the MD simulation with $\phi(r)$ reproduces the values of $S(k, \omega)$ around $\omega = 0$ and $\omega > 5$ ps^{-1} fairly well. On the other hand, the values of $S(k, \omega)$ calculated with $\phi_{ps}(r)$ are smaller than the experimental results in the low-ω region. The $S(k, \omega)$ obtained from the MD simulation with $\phi(r)$ does not show the peak around 4.5 ps^{-1}, which was observed experimentally, but decays monotonically. Next we compare $S(k, \omega)$ for $k = 1.50$ Å^{-1} with experimental data. For this k-value the dashed line is in better agreement with experimental data around $\omega = 0$. This can be understood as follows. Since, as shown in figure 2, the experimental static structure factor is scattered substantially, both the solid and dashed lines seem to agree with the experimental data within the experimental error at $k = 1.5$ Å^{-1}. However, the dashed line must be in better agreement with the 'real' static structure factor than the solid one is.

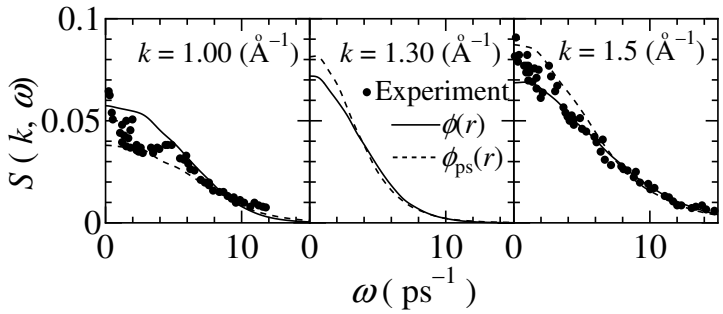

Figure 8. Dynamic structure factors $S(k, \omega)$ at 1900 K for the three wavevectors obtained by the Fourier transformation of $F(k, t)$ in figure 5. The dots are the neutron inelastic scattering results at 1873 K [4].

As for the side peak of $S(k, \omega)$ for $k = 1.0$ Å^{-1}, Pilgrim *et al* interpret it as the vibration mode of a dimer [7]. If this is the case, it is necessary to take account of several kinds of interaction: the inter-dimeric, intra-dimeric, ion–dimer and ion–ion interactions. In such a system, the pseudopotential perturbation theory and the pairwise-additive approximation may not work well. On the other hand, the effective pair potential derived from the experimental structure factor is an 'effective' pair potential, in the sense that it includes all kinds of interactions existing in a real liquid system. Therefore when a dimer exists in a liquid, the effective pair potential includes such interactions effectively. However, since the data for the experimental static structure factor $S(k)$ at 1900 K are scattered and no distinct structure implying the existence of a dimer is seen in $S(k)$, $\phi(r)$ shows little effect from a dimer, if any. To investigate whether an effective pair potential can reproduce the side peak in $S(k, \omega)$ near the critical point or not, more accurate experimental static structure data, which are used as input data in the inverse method, are necessary.

3.4. Dynamic structure for the long-wavelength region

To study the dynamic structure for a small-k region at 1900 K, we perform the MD simulation with a larger system of 8000 atoms. In this system the smallest wavenumber is 0.052 Å^{-1}. Though there are no experimental data on $S(k, \omega)$ for such a small-k region, it is considered that $\phi_{ps}(r)$ cannot reproduce the real $S(k, \omega)$ because it fails to reproduce even the static

structure factor for these k-values. Therefore we show the results for $F(k,t)$ and $S(k,\omega)$ obtained with only $\phi(r)$ in figures 9(a) and 9(b), respectively. The interesting feature is that, for $k = 0.090$ Å^{-1}, $F(k,t)$ shows oscillatory behaviour and the corresponding peak is seen in $S(k,\omega)$ at $\omega = 0.4$ ps^{-1}, while $F(k,t)$ shown in figure 5 decays monotonically and $S(k,\omega)$ shown in figure 8 has no side peak. These features become more distinct for $k = 0.052$ Å^{-1} and the clearer side peak around $\omega = 0.2$ ps^{-1} is seen in $S(k,\omega)$. This means that there exists a propagating density fluctuation with k-values smaller than about 0.1 Å^{-1} in the liquid rubidium at 1900 K.

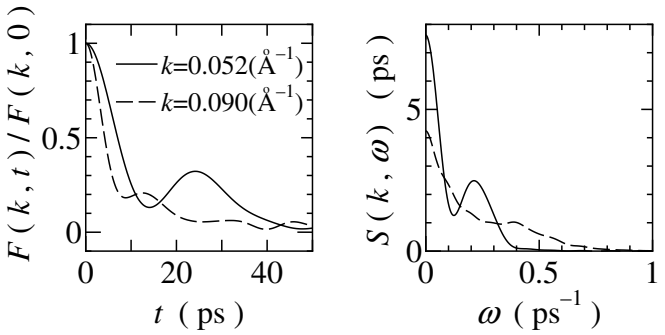

Figure 9. The normalized intermediate-scattering functions $F(k,t)/F(k,0)$ and the dynamic structure factors $S(k,\omega)$ at 1900 K for small k-values. These results are obtained with $\phi(r)$ from the MD simulation for the system of 8000 atoms.

3.5. Mean square displacements

The results for the MSD are shown in figure 10. The solid and the dashed lines are obtained with $\phi(r)$ and $\phi_{ps}(r)$, respectively. For comparison, the result calculated from an *ab initio* MD simulation by Shimojo *et al* [15] is also shown in figure 10(a) as the dashed-and-dotted line. It can be seen from figure 10(a) that the MSD is very sensitive to the effective pair potential. From the gradient of the MSD for $t \geqslant 1$ ps, where the MSD shows linear behaviour, the self-diffusion coefficients D are calculated. The values of D thus obtained for the systems with $\phi(r)$ and $\phi_{ps}(r)$ are 3.4×10^{-5} and 2.1×10^{-5} cm^2 s^{-1}, respectively. The experimental values are 2.5–3.8 $\times 10^{-5}$ cm^2 s^{-1} [33] and the result from the *ab initio* MD simulation [15] is 2.5×10^{-5} cm^2 s^{-1}. Though the value of D obtained with $\phi(r)$ seems to be in the range of these experimental data, since a measured D for a liquid system has, in general, uncertainties arising from the convection, we should discuss the result for D obtained with the calculations rather than with the experimental data. The value of D obtained with $\phi(r)$ is larger than D obtained with $\phi_{ps}(r)$ and the result from the *ab initio* MD. The reason for this is as follows. As we have pointed out, χ_T for the system of atoms interacting with $\phi(r)$ is larger than that of the real system. As a consequence, the position of the repulsive part of $\phi(r)$ is shifted further inside than that of $\phi_{ps}(r)$. That is, the effective core radius of $\phi(r)$ is too small and, as a result, the diffusion coefficient is large.

The MSD at 1700 K calculated with $\phi(r)$ and $\phi_{ps}(r)$ are shown in figure 10(b). The agreement between the two curves is very good. Both curves show the linear behaviour for $t \geqslant 2$ ps. The self-diffusion coefficients D estimated from the gradient of the MSD are 8.3 and 7.9×10^{-4} cm^2 s^{-1}, for $\phi(r)$ and $\phi_{ps}(r)$, respectively.

In figure 10(c), the MSD at 1900 K are shown. Unlike the case with the temperature of 1700 K, the two lines obtained with $\phi(r)$ and $\phi_{ps}(r)$ at 1900 K differ substantially. This

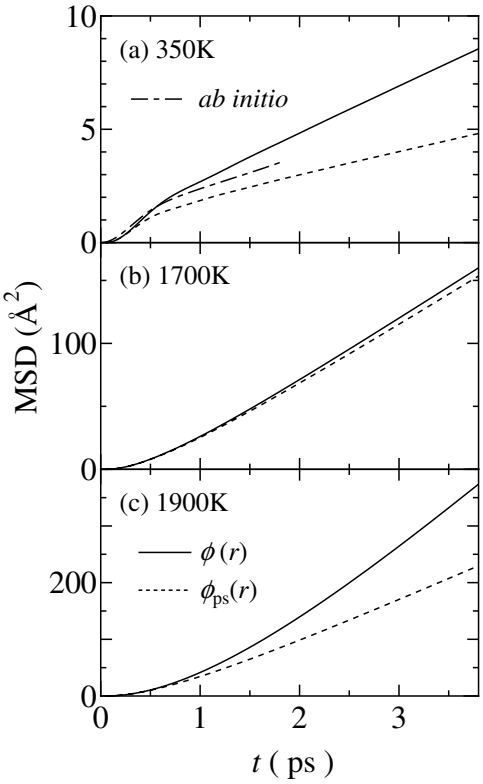

Figure 10. The mean square displacement (MSD) of atoms at (a) 350 K, (b) 1700 K and (c) 1900 K. The solid and dashed lines show the results obtained with $\phi(r)$ and $\phi_{ps}(r)$, respectively. The results from the *ab initio* MD simulation [15] are also shown, as the dashed-and-dotted line in (a).

difference between the two lines comes from the softness of the repulsive part of $\phi(r)$ as seen in figure 1. The diffusion coefficients estimated from the gradient of the MSD are 2.2×10^{-3} and 1.1×10^{-3} cm^2 s^{-1}, respectively.

3.6. Velocity autocorrelation functions

The normalized velocity autocorrelation functions $Z(t)/Z(0)$ are shown in figure 11. The solid and the dashed lines are obtained with $\phi(r)$ and $\phi_{ps}(r)$, respectively. The result from the *ab initio* MD simulation [15] is also shown as the dashed-and-dotted line at 350 K. At 350 K these curves damp with oscillation around zero. The negative value of $Z(t)$ implies a high probability of a large-angle deflection in its motion; near the triple point, since a tagged ion is enclosed in a cage formed by its neighbour ions, the ion cannot diffuse easily but vibrates in the cage for a relatively long time. Because of the stronger spatial correlation in the system of $\phi_{ps}(r)$ than that in the system of $\phi(r)$, the period of the oscillation in $Z(t)$ for $\phi_{ps}(r)$ is shorter than that for $\phi(r)$.

At 1700 K the agreement between the two curves is very good. In this thermodynamic state, $Z(t)$ does not oscillate but decays monotonically and does not take negative values. This means that the cage effect does not exist and ions can propagate over larger distances without any collision.

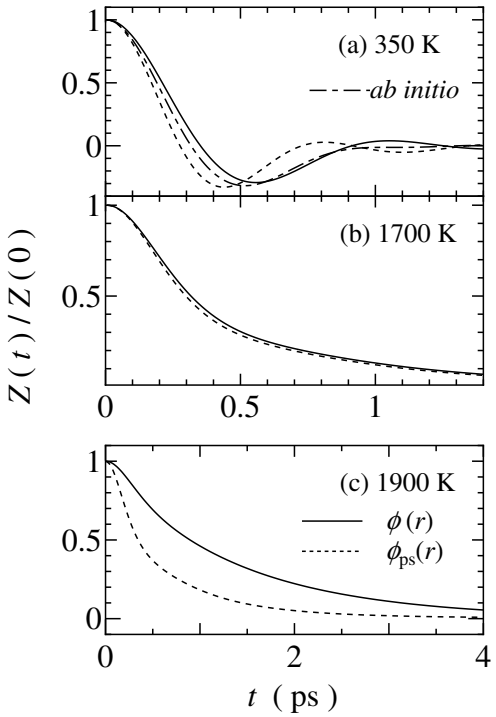

Figure 11. The velocity autocorrelation function at (a) 350 K, (b) 1700 K and (c) 1900 K. The solid and dashed lines show the results obtained with $\phi(r)$ and $\phi_{ps}(r)$, respectively. The results from the *ab initio* MD simulation [15] are also shown, as the dashed-and-dotted line in (a).

At 1900 K, unlike the case at the temperature of 1700 K, the two lines differ substantially from each other. The solid line for $Z(t)$ decays much more slowly than the dashed one. These differences come from the softness of the repulsive part of $\phi(r)$.

4. Summary

In this paper, we have investigated the dynamic structure of expanded liquid rubidium by means of MD simulation using two kinds of effective pair potential, $\phi(r)$ and $\phi_{ps}(r)$, where $\phi(r)$ is derived from the experimental static structure factor by the inverse method and $\phi_{ps}(r)$ is obtained from the pseudopotential perturbation theory.

It is found that, near the triple point, the dynamic properties for a small k are very sensitive to the effective pair potential. Therefore it is difficult to reproduce the experimental dynamic properties by MD simulation with the same accuracy as for the static structure factor in such a k-region. It is expected, however, that if more accurate experimental static structure data were available, a more accurate dynamic structure could be obtained by our method.

At the temperature of 1700 K, the dynamic structure factors $S(k, \omega)$ obtained with $\phi(r)$ can reproduce the experimental data very well. On the other hand, even if $S(k)$ calculated with $\phi_{ps}(r)$ deviates from experiment only slightly for a particular k-value, a distinct discrepancy is seen as regards the dynamic correlation functions.

Near the critical point at 1900 K, though the side peak observed in $S(k, \omega)$ for $k = 1.0$ Å^{-1} is not reproduced in the present calculation, $S(k, \omega)$ obtained with $\phi(r)$ is in fairly good

agreement with the experimental dynamic structure factor. We show for the first time that the propagating density fluctuations exist for k-values smaller than about 0.1 Å^{-1} at 1900 K.

We conclude that the effective pair potentials derived from observed static structure factors of liquid rubidium with high accuracy can reproduce the dynamic structures very well from the triple point up to near the critical point.

Acknowledgments

This work was supported by a Grant-in-Aid for Scientific Research, from the Ministry of Education, Science, Sports and Culture, Japan. We thank the Centre for Promotion of Computational Science and Engineering (CCSE) of Japan Atomic Energy Research Institute (JAERI) for allowing us to use the parallel supercomputer Fujitsu VPP300. We also acknowledge the Supercomputer Centre, Institute for Solid State Physics, University of Tokyo, for allowing us to use the Fujitsu VPP500.

References

[1] Franz G, Freyland W and Hensel F 1980 *J. Physique Coll.* **41** C8 70
[2] Hosokawa S, Pilgrim W-C, Hensel F, Hazemann J-L, Raoux D, Mezouar M, Le Bihan T and Häusermann D 1999 *J. Non-Cryst. Solids* **250–252** 159
[3] Winter R, Hensel F, Bodensteiner T and Gläser W 1987 *Ber. Bunsenges. Phys. Chem.* **91** 1327
[4] Pilgrim W-C, Winter R, Hensel F, Morkel C and Gläser W 1991 *Ber. Bunsenges. Phys. Chem.* **95** 1133
[5] Pilgrim W-C, Winter R and Hensel F 1993 *J. Phys.: Condens. Matter* **5** B183
[6] Winter R, Pilgrim W-C and Hensel F 1994 *J. Phys.: Condens. Matter* **6** A245
[7] Pilgrim W-C, Ross M, Yang L H and Hensel F 1997 *Phys. Rev. Lett.* **78** 3685
[8] Hoshino K, Matsuda N and Watabe M 1990 *J. Phys. Soc. Japan* **59** 2027
[9] Mori H, Hoshino K and Watabe M 1990 *J. Phys. Soc. Japan* **59** 3254
[10] Matsuda N, Mori H, Hoshino K and Watabe M 1991 *J. Phys.: Condens. Matter* **3** 827
[11] Hoshino K, Ugawa H and Watabe M 1992 *J. Phys. Soc. Japan* **61** 2182
[12] Hoshino K, Shimojo F and Watabe M 1994 *J. Phys. Soc. Japan* **63** 2185
[13] Kahl G and Kambayashi S 1994 *J. Phys.: Condens. Matter* **6** 10 897
[14] Kahl G 1994 *J. Phys.: Condens. Matter* **6** 10 923
[15] Shimojo F, Zempo Y, Hoshino K and Watabe M 1995 *Phys. Rev.* B **52** 9320
[16] Hoshino K and Shimojo F 1996 *J. Phys.: Condens. Matter* **8** 9315
[17] González L E, González D J, Dalgıç S and Silbert M 1999 *4th Liquid Matter Conf.* pp 3–20
[18] Munejiri S, Shimojo F, Hoshino K and Watabe M 1996 *J. Non-Cryst. Solids* **205–207** 278
[19] Munejiri S, Shimojo F, Hoshino K and Watabe M 1997 *J. Phys.: Condens. Matter* **9** 3303
[20] Reatto L, Levesque D and Weis J J 1986 *Phys. Rev.* A **33** 3451
[21] Munejiri S, Shimojo F, Hoshino K and Watabe M 1995 *J. Phys. Soc. Japan* **64** 344
[22] Dzugutov M and Dahlborg U 1989 *Phys. Rev.* A **40** 4103
[23] Munejiri S, Shimojo F and Hoshino K 1998 *J. Phys.: Condens. Matter* **10** 4963
[24] Munejiri S 1998 *PhD Thesis* Hiroshima University
[25] Hasegawa M, Hoshino K, Watabe M and Young W H 1990 *J. Non-Cryst. Solids* **117–118** 300
[26] Ichimaru S and Utsumi K 1981 *Phys. Rev.* B **24** 7385
[27] Hansen J-P and McDonald I R 1990 *Theory of Simple Liquids* 2nd edn (London: Academic)
[28] Nosé S 1984 *Mol. Phys.* **52** 255
[29] Verlet L 1968 *Phys. Rev.* **165** 201
[30] Copley J R D and Rowe J M 1974 *Phys. Rev. Lett.* **32** 49
[31] Copley J R D and Rowe J M 1974 *Phys. Rev.* A **9** 1656
[32] de Gennes P G 1959 *Physica* **25** 825
[33] Ohse W H 1985 *Handbook of Thermodynamic and Transport Properties of Alkali Metals* (Oxford: Blackwell Scientific)